

# New experimental limits on violations of the Pauli exclusion principle obtained with the Borexino Counting Test Facility

H.O. Back<sup>a</sup>, M. Balata<sup>b</sup>, A. de Bari<sup>c</sup>, A. de Bellefon<sup>d</sup>, G. Bellini<sup>e,\*a</sup>, J. Benziger<sup>f</sup>, S. Bonetti<sup>e</sup>, C. Buck<sup>g</sup>, B. Caccianiga<sup>e</sup>, L. Cadonati<sup>f,1</sup>, F. Calaprice<sup>f</sup>, G. Cecchet<sup>c</sup>, M. Chen<sup>h</sup>, A. Di Credico<sup>b</sup>, O. Dadoun<sup>d,2</sup>, D. D'Angelo<sup>i</sup>, A. Derbin<sup>j,3</sup>, M. Deutsch<sup>k,10</sup>, A. Etenko<sup>m</sup>, F. von Feilitzsch<sup>i</sup>, R. Fernholz<sup>f</sup>, R. Ford<sup>f,4</sup>, D. Franco<sup>e</sup>, B. Freudiger<sup>g,2,5</sup>, C. Galbiati<sup>f</sup>, S. Gazzana<sup>b,o</sup>, M.G. Giammarchi<sup>e</sup>, M. Goeger-Neff<sup>i</sup>, A. Goretti<sup>b</sup>, C. Grieb<sup>i</sup>, W. Hampel<sup>g</sup>, E. Harding<sup>f</sup>, F.X. Hartmann<sup>g</sup>, G. Heusser<sup>g</sup>, A. Ianni<sup>b</sup>, A.M. Ianni<sup>f</sup>, H. de Kerret<sup>d</sup>, J. Kiko<sup>g</sup>, T. Kirsten<sup>g</sup>, V.V. Kobychyev<sup>b,6</sup>, G. Korga<sup>e,7</sup>, G. Korschinek<sup>i</sup>, Y. Kozlov<sup>m</sup>, D. Kryn<sup>d</sup>, M. Laubenstein<sup>b</sup>, C. Lendvai<sup>i,2</sup>, M. Leung<sup>f</sup>, E. Litvinovich<sup>m</sup>, P. Lombardi<sup>e,o</sup>, I. Machulin<sup>m</sup>, S. Malvezzi<sup>e</sup>, J. Maneira<sup>h</sup>, I. Manno<sup>o</sup>, D. Manuzio<sup>n</sup>, G. Manuzio<sup>n</sup>, F. Masetti<sup>l</sup>, A. Martemianov<sup>m,10</sup>, U. Mazzucato<sup>l</sup>, K. McCarty<sup>f</sup>, E. Meroni<sup>e</sup>, G. Mention<sup>d</sup>, L. Miramonti<sup>e</sup>, M.E. Monzani<sup>e</sup>, V. Muratova<sup>j,3</sup>, P. Musico<sup>n</sup>, L. Niedermeier<sup>i,2</sup>, L. Oberauer<sup>i</sup>, M. Obolensky<sup>d</sup>, F. Ortica<sup>l</sup>, M. Pallavicini<sup>n</sup>, L. Papp<sup>e,7</sup>, L. Perasso<sup>e</sup>, P. Peiffer<sup>g</sup>, A. Pocar<sup>f</sup>, R.S. Raghavan<sup>p,8</sup>, G. Ranucci<sup>e,\*\*</sup>, A. Razeto<sup>n</sup>, A. Sabelnikov<sup>e</sup>, C. Salvo<sup>n,\*\*\*</sup>, R. Scardaoni<sup>e</sup>, D. Schimizzi<sup>f</sup>, S. Schoenert<sup>g</sup>, H. Simgen<sup>g</sup>, T. Shutt<sup>f</sup>, M. Skorokhvatov<sup>m</sup>, O. Smirnov<sup>j</sup>, A. Sonnenschein<sup>f,9</sup>, A. Sotnikov<sup>j</sup>, S. Sukhotin<sup>m</sup>, Y. Suvorov<sup>m</sup>, V. Tarasenkov<sup>m</sup>, R. Tartaglia<sup>b</sup>, G. Testera<sup>n</sup>, D. Vignaud<sup>d</sup>, R.B. Vogelaar<sup>a</sup>, V. Vyrodov<sup>m</sup>, M. Wojcik<sup>q</sup>, O. Zaimidoroga<sup>j</sup>, G. Zuzel<sup>g</sup>

<sup>a</sup>Physics Department, Virginia Polytechnic Institute and State University, Robeson Hall, Blacksburg, VA 24061-0435, USA

<sup>b</sup>I.N.F.N. Laboratori Nazionali del Gran Sasso, SS 17 bis Km 18+910, I-67010 Assergi(AQ), Italy

<sup>c</sup>Dipartimento di Fisica Nucleare e Teorica Università and I.N.F.N., Pavia, Via A. Bassi, 6 I-27100, Pavia, Italy

<sup>d</sup>Laboratoire de Physique Corpusculaire et Cosmologie, 11 place Marcellin Berthelot 75231 Paris Cedex 05, France

<sup>e</sup>Dipartimento di Fisica Università and I.N.F.N., Milano, Via Celoria, 16 I-20133 Milano, Italy

<sup>f</sup>Dept. of Physics, Princeton University, Jadwin Hall, Washington Rd, Princeton NJ 08544-0708, USA

<sup>g</sup>Max-Planck-Institut fuer Kernphysik, Postfach 103 980 D-69029, Heidelberg, Germany

<sup>h</sup>Dept. of Physics, Queen's University Stirling Hall, Kingston, Ontario K7L 3N6, Canada

<sup>i</sup>Technische Universität München, James Franck Strasse, E15 D-85747, Garching, Germany

<sup>j</sup>Joint Institute for Nuclear Research, 141980 Dubna, Russia

<sup>k</sup>Dept. of Physics Massachusetts Institute of Technology, Cambridge, MA 02139, USA

<sup>l</sup>Dipartimento di Chimica Università, Perugia, Via Elce di Sotto, 8 I-06123, Perugia, Italy

<sup>m</sup>RRC Kurchatov Institute, Kurchatov Sq.1, 123182 Moscow, Russia

<sup>n</sup>Dipartimento di Fisica Università and I.N.F.N., Genova, Via Dodecaneso, 33 I-16146 Genova, Italy

<sup>o</sup>KFKI-RMKI, Konkoly Thege ut 29-33 H-1121 Budapest, Hungary

<sup>p</sup>Bell Laboratories, Lucent Technologies, Murray Hill, NJ 07974-2070, USA

<sup>q</sup>M.Smoluchowski Institute of Physics, Jagellonian University, PL-30059 Krakow, Poland

22 June 2004

**Abstract.** The Pauli exclusion principle (PEP) has been tested for nucleons ( $n, p$ ) in  $^{12}\text{C}$  and  $^{16}\text{O}$  nuclei, using the results of background measurements with the prototype of the Borexino detector, the Counting Test Facility (CTF). The approach consisted of a search for  $\gamma$ ,  $n$ ,  $p$  and/or  $\alpha$ 's emitted in a non-Paulian transition of  $1P$ - shell nucleons to the filled  $1S_{1/2}$  shell in nuclei. Similarly, the Pauli-forbidden  $\beta^\pm$  decay processes were searched for. Due to the extremely low background and the large mass (4.2 tons) of the CTF detector, the following most stringent up-to-date experimental bounds on PEP violating transitions of nucleons have been established:  $\tau(^{12}\text{C} \rightarrow ^{12}\tilde{\text{C}} + \gamma) > 2.1 \cdot 10^{27}$  y,  $\tau(^{12}\text{C} \rightarrow ^{11}\tilde{\text{B}} + p) > 5.0 \cdot 10^{26}$  y,  $\tau(^{12}\text{C}(^{16}\text{O}) \rightarrow ^{11}\tilde{\text{C}}(^{15}\tilde{\text{O}}) + n) > 3.7 \cdot 10^{26}$  y,  $\tau(^{12}\text{C} \rightarrow ^8\tilde{\text{B}}e + \alpha) > 6.1 \cdot 10^{23}$  y,  $\tau(^{12}\text{C} \rightarrow ^{12}\tilde{\text{N}} + e^- + \tilde{\nu}_e) > 7.6 \cdot 10^{27}$  y and  $\tau(^{12}\text{C} \rightarrow ^{12}\tilde{\text{B}} + e^+ + \nu_e) > 7.7 \cdot 10^{27}$  y, all at 90% C.L.

**Key words.** Pauli exclusion principle – low background measurements

**PACS.** 1.1.30.-j, 24.80.+y, 23.20.-g, 27.20.+n

## 1 Introduction

The exclusion principle was formulated by W.Pauli in 1925 and in its original form postulated that only one electron with definite spin orientation can occupy each of the allowed Bohr orbits in an atom. In this way PEP explains the regularities of the Periodic Table and atomic spectra. In modern Quantum Field Theory (QFT), the PEP appears automatically for systems of identical fermions as a result of the anti-commutativity of the fermion creation and annihilation operators. Violation of the PEP, as of the nonconservation of electric charge, would contradict modern quantum field theory.

PEP has fundamental importance, but it was not extensively studied experimentally for 15 years until the electron stability was tested. Goldhaber pointed out that the same experimental data which were used to set a limit on the lifetime of the electron can be used to test the validity of the PEP for atomic electrons [1]. Pioneering experiments were performed by Reines and Sobel by searching for X-rays emitted in the transition of an L-shell electron to the filled K-shell in an atom [1], and by Logan and Ljubivic, who searched for  $\gamma$ -quanta emitted in a PEP-forbidden transition of nucleons in nuclei [2].

In 1980 Amado and Primakoff pointed out that in the framework of QFT, these PEP-violating transitions are forbidden even if PEP-violation takes place [3]. Later a theoretical models describing a violation of PEP were constructed in [4]-[6], but it was found that even small PEP-violation leads to negative probabilities for some processes [7]. Critical studies of the possible violation of PEP have been done both theoretically and experimentally by Okun [8],[9].

One of the methods of testing PEP is the search for atoms or nuclei in a non-Paulian state; another is the

search for the prompt radiation accompanying non-Paulian transitions.

Violation of PEP in the nucleon system has been studied by searching for the non-Paulian transitions with  $\gamma$ -[2],[10],[11],  $p$ -[12],[13] and  $n$ -[14] emission, non-Paulian  $\beta^+$ ,  $\beta^-$ - decays [15],[11] and in nuclear  $(p,p)$ ,  $(p,\alpha)$ -reactions on  $^{12}\text{C}$  [16].

The sensitivity of the forbidden transitions method is defined by the mass of the detector and by the background level of detector. The extremely low background level and the large mass of the CTF allowed setting new limits on the electron, neutrino and nucleon stability and neutrino electromagnetic properties [17] - [20]. The approach used in the search for nucleon and dinucleon disappearance [19] is close to the one used in the present letter to search for PEP violation.

## 2 Experimental set-up and measurements

### 2.1 Brief description of the CTF

Borexino, a real-time 300 ton detector for low-energy neutrino spectroscopy, is nearing completion in the Gran Sasso Underground Laboratory (see [21] and refs. therein). The main goal of the detector is the measurement of the  $^7\text{Be}$  solar neutrino flux via  $(\nu, e)$ - scattering in an ultra-pure liquid scintillator, but several other basic questions in astro- and particle physics will also be addressed.

CTF, installed in the Gran Sasso underground laboratory, is a prototype of the Borexino detector. Detailed reports on the CTF results were published elsewhere [21]-[23], and only the main characteristics of the set-up are outlined here.

The CTF consists of an external cylindrical water tank ( $\varnothing 11 \times 10$  m;  $\approx 1000$  t of water) serving as passive shielding for  $4.2 \text{ m}^3$  of liquid scintillator (LS) contained in a transparent nylon spherical vessel of  $\varnothing 2.0$  m. High purity water with a radio-purity of  $\approx 10^{-14}$  g/g (U/Th),  $\approx 10^{-12}$  g/g (K) and  $< 2 \mu\text{Bq/l}$  for  $^{222}\text{Rn}$  is used for the shielding. The LS was purified to the level of  $\approx 10^{-16}$  g/g in U/Th contamination.

We analyze here the data of the second phase of the CTF detector (CTF2). The liquid scintillator used at this stage was a phenylxylylethane (PXE,  $\text{C}_{16}\text{H}_{18}$ ) with p-diphenylbenzene (para-terphenyl) as a primary wavelength shifter at a concentration of 2 g/l, along with a secondary wavelength shifter 1,4-bis-(2-methylstyrol)-benzene (bis-MSB) at 20 mg/l [24]. The density of the scintillator is 0.99 kg/l. The scintillator principal de-excitation time is less than 5 ns, which permits good position reconstruction. In the CTF2 an additional nylon screen between the scintillator vessel and PMTs was installed, acting as a barrier against penetration of external radon. The water volume of the CTF2 detector is instrumented with a Čerenkov muon detector (muon veto system).

The scintillation light is collected with 100 large phototubes (PMTs) fixed to a 7- m diameter support structure placed inside the water tank. The PMTs are fitted with

<sup>a</sup> \* Spokesman

\*\* Project manager

\*\*\* Operational manager

◊ GLIMOS

◊ Detector installation manager

<sup>1</sup> Now at Massachusetts Institute of Technology, NW17-161, 175 Albany St. Cambridge, MA 02139

<sup>2</sup> Marie Curie fellowship at LNGS

<sup>3</sup> On leave of absence from St. Petersburg Nuclear Physics Inst. - Gatchina, Russia

<sup>4</sup> Now at Sudbury Neutrino Observatory, INCO Creighton Mine, P.O.Box 159 Lively, Ontario, Canada, P3Y 1M3

<sup>5</sup> Now at Institute for Nuclear Physics, Forschungszentrum Karlsruhe, Postfach 3640, 76021 Karlsruhe

<sup>6</sup> Now at Institute for Nuclear Research, Prospekt Nauki 47, MSP 03680, Kiev, Ukraine

<sup>7</sup> On leave of absence from KFKI-RMKI, Konkoly Thege ut 29-33 H-1121 Budapest, Hungary

<sup>8</sup> Present Address: Department of Physics, Virginia Polytechnic Institute and State University, Blacksburg VA 24061

<sup>9</sup> Center for Cosmological Physics, University of Chicago, 933 E. 56<sup>th</sup> St., Chicago, IL 60637

<sup>10</sup> Deceased

Correspondence to: derbin@mail.pnpi.spb.ru (A.Derbin)  
smirnov@lngs.infn.it (O.Smirnov)

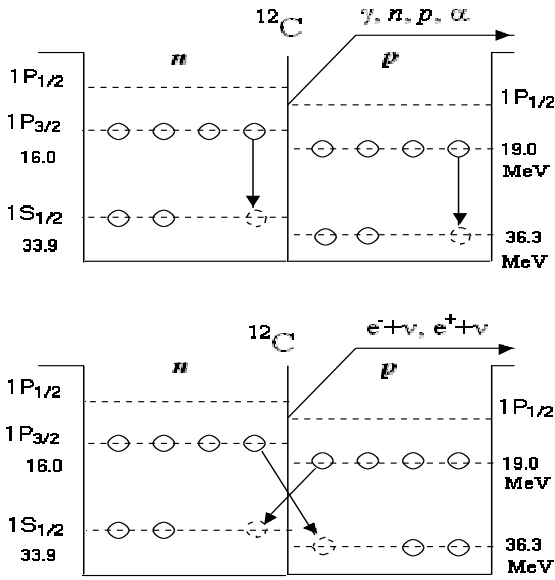


**Fig. 1.** Occupation of energy levels by protons and neutrons for the  $^{12}\text{C}$  ground state in a simple shell model. Schemes of non-Paulian transitions of nucleons from the  $P$ -shell to the filled  $S$ -shell: a) with  $\gamma$ -,  $n$ -,  $p$ - and  $\alpha$ -emission; b) with  $\beta^+$ -,  $\beta^-$ -emission.

light concentrators which provide a total optical coverage of 21%.

For each event the charge and time of every PMT hit are recorded. Each electronics channel is supported by an auxiliary channel used to record events coming within a time window of 8.2 ms after the trigger, which allows tagging of fast time-correlated events with a decrease of the overall dead time of the detector. For longer delays, the computer clock is used, providing an accuracy of  $\approx 50$  ms. Event parameters measured in the CTF2 include the total charge collected by the PMTs during the 0–500 ns window, used to determine an event’s energy; the charge in the ‘tail’ of the pulse (48–548 ns) which is used to distinguish between  $\alpha$  and  $\beta$  events through the pulse shape discrimination method; PMT timing, used to reconstruct the event’s position; and the time elapsed between sequential events, used to tag time-correlated events.

## 2.2 Detector calibration

The energy of an event in the CTF detector is measured using the total collected charge from all PMT’s. In a simple approach, the response of the detector is assumed to be linear with respect to the energy released in the scintillator. The coefficient  $A$  linking the event energy and the total collected charge is called the light yield (or photoelectron yield). Practically, the light yield for electrons can be considered linear in energy only above  $\sim 1$  MeV. At low energies the phenomenon of “ionization quenching”

violates the linear dependence of the light yield versus energy. The deviations from the linearity can be taken into account by the ionization deficit function  $f(k_B, E)$ , where  $k_B$  is the empirical Birks’ constant [25]. For the calculation of the ionization quenching effect for the PXE scintillator, we used the KB program from the CPC library [26].

The ionization quenching effect leads to a shift in the position of the total absorption peak for  $\gamma$ ’s on the energy scale calibrated using electrons. In fact, the position of the 1461 keV  $^{40}\text{K}$   $\gamma$  in the CTF2 data corresponds to 1360 keV of energy deposited by an electron [18].

The energy calibration derived from the  $^{14}\text{C}$   $\beta$ -spectrum gives  $A = 3.72 \pm 0.08$  photoelectrons/(MeV  $\times$  PMT) for high energy electrons depositing their energy at the detector’s center.<sup>1</sup>

The detector energy and spatial resolution were studied with radioactive sources placed at different positions inside the active volume of the CTF2. A typical spatial  $1\sigma$  resolution is 10 cm at 1 MeV. The studies showed also that the total charge response of the detector can be approximated by a Gaussian. For energies  $E \geq 1$  MeV (which are of interest here), the relative resolution can be expressed as  $\sigma_E/E = \sqrt{3.8 \text{ keV}/E + 2.3 \cdot 10^{-3}}$  [27] for events uniformly distributed over the detector’s volume.

The energy dependence on the collected charge becomes non-linear for energies  $E \geq 5$  MeV because of the saturation of the ADCs used. In this region we are using only the fact of whether or not candidate events are observed, hence the mentioned nonlinearity doesn’t influence the result of the analysis.

More details on the energy and spatial resolutions of the CTF and ionization quenching for electrons,  $\gamma$  quanta and  $\alpha$  particles were reported in [17],[18],[27].

## 2.3 Muon veto

The CTF2 was equipped with a water Čerenkov muon veto system. It consists of 2 concentric rings of 8 PMTs each, installed at the bottom of the tank. The radii of the rings are 2.4 and 4.8 m. Muon veto PMTs look upward and have no light concentrators. The muon veto system was optimized in order to have a negligible probability of registering the scintillation events in the 250–800 keV  $^7\text{Be}$  neutrino energy region. The behaviour of the muon veto has been specially studied at higher energies [19]. Experimental measurements with a radioactive source (chain of  $^{222}\text{Rn}$ ) [28] gave the value  $\eta(E) = (1 \pm 0.2)\%$  in the 1.8–2.0 MeV region for the probability  $\eta(E)$  of identification of a scintillation event with energy  $E$  in the LS as a muon. The energy dependence of  $\eta(E)$  was also calculated by a ray-tracing Monte Carlo method accounting for specific

<sup>1</sup> No measurements with high energy monoenergetic electrons are available for the PXE scintillator. This is just convenient interpolation of the value obtained fitting  $^{14}\text{C}$  spectrum, which allows to separate energy dependent part using ionization deficit function  $f(k_B, E)$ . The registered amount of light at any energy can be calculated as  $Y(E) = A \cdot f(k_B, E)$ . For 1 Mev electron  $Y(1 \text{ MeV}) = 3.54 \pm 0.08$  p.e./ (MeV  $\times$  PMT).

features of the light propagation in the CTF2 which are detailed in [23]. The calculated function was adjusted to reproduce correctly the experimental measurements with the  $^{222}\text{Rn}$  source.

### 3 Data analysis

#### 3.1 Theoretical considerations

The non-Paulian transitions were searched for in nuclei of  $^{12}\text{C}$  contained in the scintillator and  $^{16}\text{O}$  in the water shield of the CTF2 detector, respectively. The nucleon level scheme of  $^{12}\text{C}$  in a simple shell model is shown in Fig.1. The nucleon binding energies for the light nuclei ( $^{12}\text{C}$ ,  $^{16}\text{O}$  and others) were measured while studying  $(p, 2p)$  and  $(p, np)$  proton scattering reactions with 1 GeV energy [29]. The measured values for  $1S_{1/2}$  and  $1P_{3/2}$  shells [29] together with  $n, p$  and  $\alpha$  separation energies [30] are shown in table 1. For example, the measured values for the  $1S_{1/2}$  shell of  $^{12}\text{C}$  are  $E_n(1S_{1/2}, ^{12}\text{C}) = 36.3 \pm 0.6$  MeV and  $E_p(1S_{1/2}, ^{12}\text{C}) = 33.9 \pm 0.9$  MeV. These values significantly differ from value  $E_p(1S_{1/2}, ^{12}\text{C}) = 39 \pm 1$  MeV extracted from  $(e, ep)$ -scattering [31].

**Table 1.** The separation energy  $S_p, S_n, S_\alpha$  [30], the nucleon binding energy (with errors) of the  $1P_{3/2}$  and  $1S_{1/2}$  shells [29], and the nuclear binding energy  $E_b$  (keV)[30].

	$^9\text{Be}$	$^{11}\text{B}$	$^{12}\text{C}$	$^{16}\text{O}$
$S_p$	16.9	11.2	16.0	12.3
$S_n$	1.66	10.7	18.7	15.7
$S_\alpha$	2.5	8.7	7.4	7.2
$1P_{3/2}(p)$	17.0 (0.2)	17.5 (0.5)	16.0 (0.2)	18.0 (0.3)
$1P_{3/2}(n)$	18.1 (0.5)	18.4 (0.6)	19.0 (0.3)	22.0 (0.4)
$1S_{1/2}(p)$	27.7 (0.5)	33.5 (0.9)	33.9 (0.9)	39.8 (0.9)
$1S_{1/2}(n)$	29.2 (0.8)	34.5 (1.0)	36.3 (0.6)	42.2 (1.0)
$E_b$	58164.9	76204.8	92161.8	127619.3

The transition of a nucleon from the  $P$ -shell to the filled  $S$ -shell will result in excited nuclei  $^{12}\text{C}$ . The excitation energy corresponds to the difference of the binding energies of nucleons on  $S$ - and  $P$ -shells. As one can see from the table, the energy release in the non-Paulian transitions in  $^{12}\text{C}$  and  $^{16}\text{O}$  is comparable with separation energies  $S_p, S_n, S_\alpha$ ; hence, together with emission of  $\gamma$ -quanta, the emission of  $n, p$  and  $\alpha$  is possible. Because of the uncertainties in the values of  $E_{S_{1/2}}^{n,p}$ , the prediction of the branching ratio for the emission in each of the above mentioned channels has a poor significance. For the case of the nucleon and dinucleon invisible decay in nuclei, the branching ratio and spectra of the emitted particles were considered in [32]. In the present paper we give the separate limits on the probabilities for each of the possible reactions. The weak processes with a violation of the PEP ( $\beta^+, \beta^-$ -decays) [11], [15] with a non-Paulian nucleon in the final state (on  $1S_{1/2}$  shell) are considered as well.

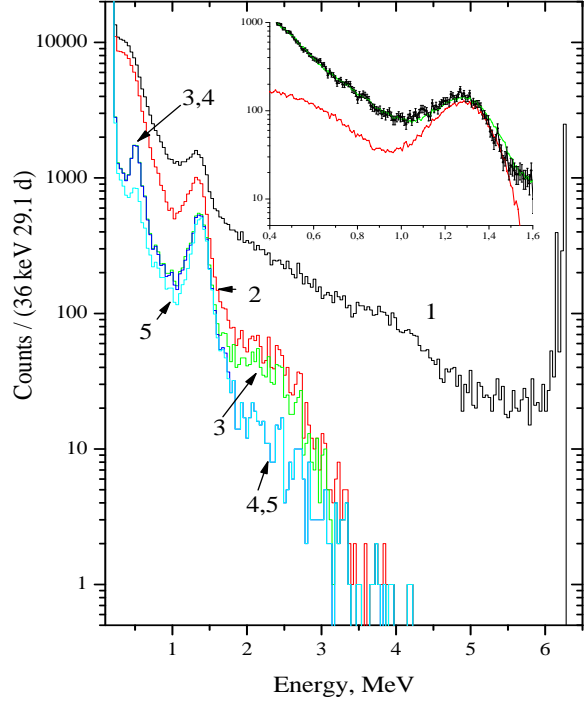


**Fig. 2.** Background energy spectra of the 4.2 ton Borexino CTF2 detector measured over 29.1 days. From top to bottom: (1) the raw spectrum; (2) with muon veto cut; (3) non-muon events inside the radius  $R \leq 100$  cm; (4) pairs of correlated events (with time interval  $\Delta t \leq 8.2$  ms between signals) are removed; (5)  $\alpha/\beta$  discrimination is applied to eliminate any contribution from  $\alpha$  particles. In the inset, the simulated response function for external  $^{40}\text{K}$   $\gamma$ 's is shown together with the experimental data.

#### 3.2 Data selection

The candidate events, relevant for our studies, have to satisfy the following criteria: (1) the event should occur in the volume of the detector and must not be accompanied by the muon veto tag; the probability of detecting high energy events in LS has to be taken into account; (2) it should be single (not followed by a time-correlated event) except in the case of neutron emission; (3) its pulse shape must correspond to that of events caused by  $\gamma, \beta$  or  $\alpha$  particles depending on the specific channel under study.

The experimental energy spectrum in CTF2, accumulated during 29.1 days of measurements (live time), is shown in fig. 2. The trigger level was set at 21 fired PMT in a 30 ns window; the total count rate at this threshold was  $0.5 \text{ s}^{-1}$ . The raw spectrum is presented on the top. The peak at 1.46 MeV, present in all spectra, is due to  $\gamma$ -quanta from  $^{40}\text{K}$  decays outside the scintillator, mainly in the ropes supporting the nylon sphere. The peak-like structure at  $\sim 6.2$  MeV is caused by saturation of the electronics by high-energy events.

The second spectrum is obtained by applying the muon cut, which suppressed the background rate by up to two orders of magnitude, depending on the energy region. No

events with energy higher than 4.5 MeV passed this cut. In the next stage of the data selection we applied a cut on the reconstructed radius. We used a  $R \leq 100$  cm (radius of the inner vessel) cut aiming to reduce significantly the surface background events (mainly due to the  $^{40}\text{K}$  decays outside the inner vessel) and leave the events uniformly distributed over the detector volume. The efficiency of the cut has been studied with MC simulation and lies in the range of  $\epsilon_R = 0.76 - 0.80$  in the energy region 1–2 MeV. The time-correlated events (occurring in the time window  $\Delta t \leq 8.2$  ms) were also removed (spectrum 4). Suppression of non-correlated events is negligible (0.4%) due to low count rate. Additional  $\alpha/\beta$  discrimination [22] was applied to eliminate contribution from  $\alpha$  particles (spectrum 5 in fig. 2). The loss of  $\beta$ -particles for  $\alpha$  identification efficiency 85% is less than 2% for the 1 MeV energy region [24].

The selection and treatment of data (spatial cuts, analysis of an event's pulse shape to distinguish between electrons and  $\alpha$  particles, suppression of external background by the muon veto system, etc.) is similar to that in ref. [17],[18], [19],[20].

### 3.3 Simulation of the response functions

Due to the complex phenomena of light propagation in a large volume scintillator detector, the precise modeling of the detector response is a complicated task. Among the problems, it is worth mentioning the wavelength dependence of the processes involved in light propagation; reflection/refraction on the scintillator/water interface; the light reflection on the concentrators; etc. [23]. The non-spherical shape of the inner vessel, deformed by the supporting strings, is an additional source of uncertainty. The need to follow each of the 12000 photons emitted per 1 MeV electron event makes tracing MC code very slow.

We developed a fast reliable code, based on the measurements with the detector. The perfect sets of data for the code tuning are the  $^{14}\text{C}$   $\beta$ -decay data and the easily identified  $\alpha$ 's from the radon decay in the scintillator volume. The code has two parts: the electron-gamma shower simulation (EG code) and the simulation of the registered charge and position (REG code). The EG code generates a random-position event with a random initial direction (for  $\gamma$ 's) and follows the gamma-electron shower using the EGS-4 code[33]. The low-energy  $e$  and  $\alpha$  are not propagated in the program and are considered to be point-like, with the position at the initial coordinates.

The mean registered charge corresponding to the electron's energy  $E_e$  is calculated by

$$Q_e = A \cdot E_e \cdot f(k_B, E_e) \cdot f_R(r), \quad (1)$$

where  $f_R(r)$  is a radial factor taking into account the dependence of the registered charge on the distance from the detector's center, and  $f(k_B, E_e)$  is the quenching factor for electrons. The method used to obtain  $f_R(r)$  is described in [34].

From the analysis of the PXE data, the quenching factor  $k_B = (1.5 \pm 0.1) \cdot 10^{-3}$  was found to satisfy experimental

data [18]. The value is in agreement with the high statistics fit of the  $^{14}\text{C}$   $\beta$ -spectrum. The presence of the strong  $\gamma$  line of 1.46 MeV in the CTF2 data was used to check the method: first, the quenching factor was extracted from the  $^{14}\text{C}$   $\beta$ -spectrum, and then the  $^{40}\text{K}$   $\gamma$ 's were simulated. The position of the peak in the model agreed with the real data to within 1% accuracy.

The mean registered charge corresponding to the  $\alpha$  of energy  $E_\alpha$  is calculated by

$$Q_\alpha = A \cdot E_\alpha \cdot f_\alpha(E_\alpha) \cdot f_R(r), \quad (2)$$

where  $f_\alpha(E_\alpha)$  is the quenching factor for  $\alpha$ 's. The following approximation of the quenching factor  $f_\alpha(E_\alpha)$  was found on the basis of laboratory measurements for a scintillator based on pseudocumene (PC):

$$f_\alpha^{PC}(E_\alpha) = \frac{1}{a - b \cdot E_\alpha}. \quad (3)$$

with  $a = 20.4$  and  $b = 1.3$ . The measurements of the  $f_\alpha(E_\alpha)$  for PXE were performed in laboratory [35] and analyzing delayed spectra of the CTF2 [24]. It was found that an  $\alpha$ -particle with energy 7.69 MeV is quenched to an equivalent  $\beta$ -energy of  $950 \pm 12$  keV. Other reference points were found using the peaks corresponding to 3  $\alpha$ -particle of 5.3, 5.49 and 6.02 MeV correspondingly. Using the same form of approximation as for PC, we found  $a = 16.2$  and  $b = 1.1$  for the PXE scintillator.

The  $\gamma$ 's were propagated using EGS-4 code [33]. As soon as an electron of energy  $E_e$  is to appear inside the scintillator, the corresponding charge is calculated:

$$\Delta Q_i = A \cdot E_{e_i} \cdot f(k_B, E_{e_i}) \cdot f_R(r_i); \quad (4)$$

total mean collected charge is defined when the  $\gamma$  is discarded by the EG code, summing individual deposits:

$$Q_\gamma = \sum \Delta Q_i. \quad (5)$$

The weighted position is assigned to the final  $\gamma$ :

$$x_w = \frac{\sum \Delta Q_i \cdot x_i}{\sum \Delta Q_i}, \quad (6)$$

where  $\Delta Q_i$  and  $x_i$  are the charge deposited for the  $i^{\text{th}}$  electron at the position  $(x_i, y_i, z_i)$ . The analogous rule is applied for the  $y_w$  and  $z_w$  coordinates.

In the next step a random charge is generated in accordance to the normal distribution with a mean value of  $Q = \sum \Delta Q$  and with variance  $\sigma_Q = \sqrt{(1 + \overline{v_1}) \cdot Q}$ . The instrumental parameter  $\overline{v_1}$  is the relative variance of the single photoelectron charge response averaged over all PMTs of the detector. It was defined independently from the measurements with radon source inserted in the detector and from averaging the relative variances of the single photoelectron response obtained during the acceptance tests [27]. Both method give  $\overline{v_1} = 0.34 \pm 0.01$ .

Finally, the radial reconstruction is simulated taking into account energy dependence of the reconstruction precision. It is assumed that the reconstruction precision is

defined by the number of PMTs fired in an event and that reconstruction precision doesn't depend on the position. These two facts are in agreement with the measurements using the artificial radon source inserted in the CTF1 and CTF2 detectors [22].

The fit of the radial distribution of the  $\alpha$ -particle events with energy  $E_\alpha=7.69$  MeV (equivalent electron energy  $E_e=950$  keV) gives  $\sigma_R = 13.8$  cm. If we assume that the reconstruction precision is defined by the mean number  $N$  of fired channels, then the  $\sigma_R(E)$  for an event of energy  $E$  is:

$$\sigma_R(E) = \sigma_R(950 \text{ keV}) \cdot \sqrt{\frac{N(950 \text{ keV})}{\langle N(E) \rangle}}. \quad (7)$$

where mean number of fired PMTs for  $E=950$  keV is  $N(950 \text{ keV}) = 91$  (of the total 100). The number of the fired channels  $N(E)$  was simulated for every event assuming a Poisson distribution of photoelectrons registered on each PMT.

## 4 Results

### 4.1 Limits on non-Paulian transitions in $^{12}\text{C}$ and $^{16}\text{O}$ with emission of $\gamma$ .

As follows from table 1, the energy difference for the nucleon transition from the shell  $1P_{3/2}$  to the shell  $1S_{1/2}$  is  $\simeq 17.5$  MeV for  $^{12}\text{C}$ . The response functions of the CTF2 to the  $\gamma$  of this energy were simulated by the MC methods described in the previous subsection. The energy difference for the same transition in the case of  $^{16}\text{O}$  corresponds to  $\simeq 21$  MeV. The uniformly distributed  $\gamma$ 's of this energy were simulated in the 1 m- thick layer of water surrounding the scintillator. Both response functions are shown in Fig. 3 before and after the muon veto suppression.

The limit on the probability of transitions  $^{12}\text{C} \rightarrow ^{12}\tilde{\text{C}} + \gamma$  and  $^{16}\text{O} \rightarrow ^{16}\tilde{\text{O}} + \gamma$  violating the PEP are based on the experimental fact of observing no events with energy higher than 4.5 MeV passing muon veto cut. The lower limit on PEP violating transitions of nucleons from  $P$ -shell to the occupied  $1S_{1/2}$ -shell was obtained using the formula

$$\tau \geq \varepsilon_{\Delta E} \frac{N_N N_n}{S_{lim}} T, \quad (8)$$

where  $\varepsilon_{\Delta E}$  is the efficiency of registering an event in the energy interval  $\Delta E$ ,  $N_N$  is the number of nuclei under consideration,  $N_n$  is the number of nucleons ( $n$  and/or  $p$ ) in the nuclei for which the non-Paulian transitions are possible,  $T$  is the total time of measurements, and  $S_{lim}$  is the upper limit on the number of candidate events registered in the  $\Delta E$  energy interval and corresponding to the chosen confidence level.

The efficiency of 17.5 MeV  $\gamma$  detection  $\varepsilon_{\Delta E} = 4.3 \cdot 10^{-2}$  was determined in a MC simulation, taking into account the suppression of the high energy events by the muon veto system (fig. 3). The number of  $^{12}\text{C}$  target nuclei in 4.17 tonnes of liquid scintillator based on PXE is  $N_N =$

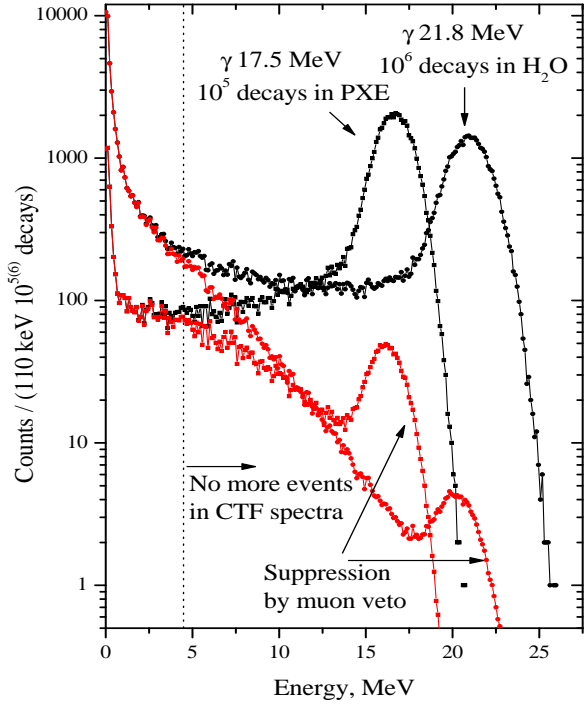


**Fig. 3.** The expected response functions of the detector for  $^{12}\text{C} \rightarrow ^{12}\tilde{\text{C}} + \gamma$  decays in the liquid scintillator and  $^{16}\text{O} \rightarrow ^{16}\tilde{\text{O}} + \gamma$  decays in the water shield before and after muon veto suppression are shown.

$1.89 \cdot 10^{29}$  (taking into account the isotopic abundance of  $^{12}\text{C}$ ). The number of nucleons on the  $P$ -shell is  $N_n = 8$ , the total data taking time is  $T = 0.080$  y, and the upper limit on the number of candidate events is  $S_{lim} = 2.44$  with 90% C.L. in accordance with the Feldman-Cousins procedure [36], recommended by the Particle Data Group.

The  $^{16}\text{O}$  nucleus has 8 nucleons on its  $1P_{3/2}$  and 4 nucleons on its  $1P_{1/2}$  shell. The values of the binding energy of the nucleons on  $1P_{1/2}$ -shell are  $E_p(1P_{1/2}) = 13.4 \pm 0.4$  MeV and  $E_n(1P_{1/2}) = 16.2 \pm 0.3$  MeV [29]. The values of  $\varepsilon_{\Delta E}$  were calculated for  $E_\gamma = 21.8$  MeV, 26 MeV ( $1P_{3/2} \rightarrow 1S_{1/2}, 1P_{1/2} \rightarrow 1S_{1/2}$  transitions) and for the two  $\gamma$ -quanta in the cascade  $E_\gamma = 21 + 5$  MeV. These values are  $5.7 \cdot 10^{-3}$ ,  $5.4 \cdot 10^{-3}$ , and  $2.2 \cdot 10^{-2}$  correspondingly. Because of the unknown branching ratio, the worst possible total efficiency  $\varepsilon_{\Delta E} = 5.6 \cdot 10^{-3}$  was adopted. The number of target  $^{16}\text{O}$  nuclei in the 1 meter thick layer of water shielding is  $N_N = 9.8 \cdot 10^{29}$  and the upper limit on the number of the candidate events corresponding to the 90% c.l. is the same as in the previous case,  $S_{lim} = 2.44$ . The limits obtained using the cited numbers are:

$$\tau(^{12}\text{C} \rightarrow ^{12}\tilde{\text{C}} + \gamma) \geq 2.1 \cdot 10^{27} \text{ y}, \quad (9)$$

$$\tau(^{16}\text{O} \rightarrow ^{16}\tilde{\text{O}} + \gamma) \geq 2.1 \cdot 10^{27} \text{ y}, \quad (10)$$

with a combined limit of  $\tau \geq 4.2 \cdot 10^{27} \text{ y}$  for the 90% c.l. This result is stronger than the ones obtained with the NEMO-2 detector  $\tau(^{12}\text{C} \rightarrow ^{12}\tilde{\text{C}} + \gamma) \geq 4.2 \cdot 10^{24} \text{ y}$  [11], and

the Kamiokande detector  $\tau(^{16}\text{O} \rightarrow ^{16}\tilde{\text{O}} + \gamma) \geq 2.7 \cdot 10^{27}$  y [10].

#### 4.2 Limits on non-Paulian transitions in $^{12}\text{C}$ with proton emission $^{12}\text{C} \rightarrow ^{11}\tilde{\text{B}} + p$ .

Energy released in these transitions is the difference between the binding energies of the final and initial nuclei:

$$Q(^{12}\text{C} \rightarrow ^{11}\tilde{\text{B}} + p) = M(^{12}\text{C}) - M(^{11}\tilde{\text{B}}) - m_p = -E_b(^{12}\text{C}) + E_b(^{11}\tilde{\text{B}}); \quad (11)$$

with the evident notations. The binding energy of the non-Paulian nuclei with 3 neutrons  $E_b(^{11}\tilde{\text{B}}_n)$  or 3 protons  $E_b(^{11}\tilde{\text{B}}_p)$  on the S-shell can be evaluated considering the binding energy  $E_b(^{11}\text{B})$  and the difference between the binding energies of nucleons on the S-shell  $E_{n,p}(S_{1/2})$  and the binding energy of the last nucleon  $S_{n,p}(^{11}\text{B})$ :

$$E_b(^{11}\tilde{\text{B}}_{n,p}) \simeq E_b(^{11}\text{B}) + E_{n,p}(1S_{1/2}) - S_{n,p}(^{11}\text{B}). \quad (12)$$

Using the data of Table 1, one can obtain  $Q(^{12}\text{C} \rightarrow ^{11}\tilde{\text{B}}_p + p) = 6.3$  MeV and  $Q(^{12}\text{C} \rightarrow ^{11}\tilde{\text{B}}_n + p) = 7.8$  MeV. Taking into account the recoil energy of the nuclei and experimental errors of  $E_{n,p}(S_{1/2})$  from table 2, the energy of the proton released in these non-Paulian transitions is  $E_p = 5.8(7.2) \pm 1.0$  MeV.

The light yield for the protons in the range of 0.6-6.0 MeV was measured for the NE213 scintillator using recoil protons from the  $(n, p)$  elastic scattering [37]. The measured data were approximated by the formula relating energy release of protons  $E_p$  and electrons  $E_e$ :

$$E_e = 0.034 \cdot E_p^2 + 0.311 \cdot E_p - 0.109 \quad (13)$$

The light yield for a proton with energy  $E_p = 5.8(7.2)$  MeV corresponds to an electron energy of  $E_e = 2.8(3.9) \pm 0.5$  MeV. It means that the proton peak can be found in the energy interval 2.0-4.7 MeV with 90% probability. The uncertainty of the peak position is few times higher than energy resolution of CTF2 ( $\sigma_E = 130$  keV for  $E_e = 2$  MeV) and covers errors due to using NE213 data instead of that for PXE.

To establish limits on the probability of these non-Paulian transitions in  $^{12}\text{C}$ , we use the formula (8). Because of uncertainty in the  $p$  peak position,  $S_{lim}$  was determined using a very conservative approach: it was defined as the number of events  $N$  inside the  $2\sigma_E$  window ( $\varepsilon_{\Delta E} = 0.68$ ) which can be excluded at a given confidence level ( $N + 1.28\sqrt{N}$  for 90% c.l.). This procedure was used for the wide energy interval 2.0-4.7 MeV. The maximum value of  $S_{lim} = 130$  at 90% c.l. (and the least stringent limit on life-time) was obtained for the energy interval 2.0-2.26 MeV. The lower limit on the life-time was found from formula (8) taking into account the efficiency of radial cut  $\varepsilon_R = 0.8$ :

$$\tau(^{12}\text{C} \rightarrow ^{11}\tilde{\text{B}} + p) \geq 5.0 \cdot 10^{26} \text{ y (90\% c.l.)}. \quad (14)$$

This result is stronger than ones obtained with the 300 kg NaI ELEGANT V detector  $\tau(^{23}\text{Na}, ^{127}\text{I} \rightarrow ^{22}\tilde{\text{N}}e, ^{126}\tilde{\text{T}}e + p) \geq 1.7 \cdot 10^{25}$  y (90% c.l.) for protons with  $E_p \geq 18$  MeV, and with the 100 kg NaI DAMA detector  $\tau(^{23}\text{Na}, ^{127}\text{I} \rightarrow ^{22}\tilde{\text{N}}e, ^{127}\tilde{\text{T}}e + p) \geq (7-9) \cdot 10^{24}$  y (90% c.l.) for protons with  $E_p \geq 10$  MeV.

#### 4.3 Limits on non-Paulian transitions in $^{12}\text{C}$ with $\alpha$ -particle emission $^{12}\text{C} \rightarrow ^8\tilde{\text{B}}e + \alpha$ .

The binding energy of an  $\alpha$ -particle in  $^{12}\text{C}$  nuclei is as low as 7.4 MeV. The energy released in the transition is the difference between the binding energies of the final and initial nuclei:

$$Q(^{12}\text{C} \rightarrow ^8\tilde{\text{B}}e + \alpha) = -E_b(^{12}\text{C}) + E_b(^8\tilde{\text{B}}e) + E_b(^4\text{He}). \quad (15)$$

The binding energy of nucleons on the S-shell of  $^8\tilde{\text{B}}e$  can be obtained using experimental values  $E_{n,p}(1S_{1/2})$  for the isotope  $^9\text{Be}$ . The binding energies for the non-Paulian nuclei  $^8\tilde{\text{B}}e_n$  and  $^8\tilde{\text{B}}e_p$  calculated thus give values  $Q \simeq 2.9 \pm 0.9$  MeV and  $Q \simeq 3.0 \pm 0.6$ , respectively. As the result, the  $\alpha$ -particles from the decay can be found in the energy interval 1.0 - 3.0 MeV with 90% probability. In accordance with (3), the light yield for an  $\alpha$  with energy between 1.0-3.0 MeV corresponds to an electron in the energy range 70 - 230 keV. The CTF2 efficiency of  $\alpha/\beta$  discrimination was not studied in this energy region and  $\alpha/\beta$  selection was not used for reaction (15). The dominant part of the background in this range is the  $\beta$ -activity of  $^{14}\text{C}$ . For the energy window ( $230 \text{ keV} \pm \sigma_E$ ,  $\sigma_E = 30$  keV) the value  $S_{lim}$  is 3400 at 90% c.l (spectrum 4 on fig. 2). Taking into account the efficiency of the radial cut  $\varepsilon_R = 0.67$ , the lower limit on lifetime for decay (15) is  $\tau \geq 1.6 \cdot 10^{25}$  y. Our results on electron stability, obtained on the same experimental data, can be used to set stronger limit on the peak near the endpoint of the  $\beta$ -spectrum [17].

For an  $\alpha$ -particle with  $E_\alpha = 1$  MeV ( $E_e = 70$  keV) the limit is weaker. Measurements with low threshold (6 fired PMTs, or  $\approx 20$  keV) were performed with 3 tons of PXE. The dead time of the system with this low threshold was 43%. At the energy 70 keV, the number of counts in the  $\beta$ -spectrum in the interval  $2\sigma_E$  is  $(6.6 \pm 0.2) \cdot 10^4 \text{ d}^{-1}$ , where error of about 3% includes both systematic and statistic effects [24]. For values  $S_{lim} = 3.3 \cdot 10^3$ ,  $\varepsilon_{\Delta E} = 0.68$ ,  $N_N = 1.35 \cdot 10^{29}$  and  $T = 2.74 \cdot 10^{-3}$  y, one can obtain

$$\tau(^{12}\text{C} \rightarrow ^8\tilde{\text{B}}e + \alpha) \geq 6.1 \cdot 10^{23} \text{ y (90\% c.l.)}. \quad (16)$$

#### 4.4 Limits on non-Paulian transitions in $^{12}\text{C}$ and $^{16}\text{O}$ with neutron emission: $^{12}\text{C} \rightarrow ^{11}\tilde{\text{C}} + n$ , $^{16}\text{O} \rightarrow ^{15}\tilde{\text{O}} + n$ .

The energy released in the decay  $^{12}\text{C} \rightarrow ^{11}\tilde{\text{C}} + n$  is equal to the difference of the binding energies of  $^{12}\text{C}$  and  $^{11}\tilde{\text{C}}$ :

$$Q(^{12}\text{C} \rightarrow ^{11}\tilde{\text{C}} + n) = -E_b(^{12}\text{C}) + E_b(^{11}\tilde{\text{C}}). \quad (17)$$

The binding energy of non-Paulian nuclei  $^{11}\tilde{C}$  can be defined as  $E_b(^{11}\tilde{C}) \simeq E_b(^{11}C) + E_{n,p}(S_{1/2}, ^{11}C) - S_{n,p}(^{11}C)$ . The nucleus  $^{11}C$  is unstable. Its nucleon separation energies are  $S_n=13.1$  and  $S_p = 8.7$  MeV. If one assumes that the binding energies of the nucleons of  $^{11}C$  on the  $S_{1/2}$  shell are close to those of  $^{12}C$  nuclei, then the energies released in the process (17) are  $Q = 6.5$  and  $4.5$  MeV for the nuclei  $^{11}\tilde{C}_p$  and  $^{11}\tilde{C}_n$  in their final states, respectively. For decays in the water, the mean neutron energy defined in the analogous way is  $\simeq 18$  MeV.

The resulting neutrons are thermalized in hydrogen-rich media (organic scintillator or water). The lifetime of neutrons in water and/or scintillator is the order of some hundreds of  $\mu s$ , after which they are captured by protons. The cross section for capture on a proton for a thermal neutron is 0.3 barns. The cross sections are much smaller for capture on the  $^{16}O$  and  $^{12}C$  nuclei:  $\sigma_c(^{12}C)=3.5$  mbarns and  $\sigma_c(^{16}O)=0.2$  mbarns. Capture of thermal neutrons  $n + p \rightarrow d + \gamma$  is followed by  $\gamma$ - emission with 2.2 MeV energy. The background levels measured in CTF2 at this energy have been used to obtain an upper limit on the number of  $\gamma$ 's with 2.2 MeV energy, and as a result, a limit on the probability of neutron production in the reactions  $^{12}C \rightarrow ^{11}\tilde{C} + n$ ,  $^{16}O \rightarrow ^{15}\tilde{O} + n$ . Protons scattered during the thermalization with energies of some MeV can be registered by the detector, hence the sequential events were not cut out in the data selection. As a result, the main contribution to the background in the 2 MeV region was attributed to the decays  $^{214}Bi \rightarrow ^{214}Po$  that were not suppressed by the delayed coincidence cut (see Fig. 4).

The analysis was made under the assumption that the mean lifetime of the nucleons is the same in  $^{12}C$  and  $^{16}O$  nuclei, and that  $n$ -emission decays within both of them contribute to the experimental spectrum simultaneously. The density of the PXE scintillator practically matches that of water. The density of nucleons that can cause the non-Paulian transitions with neutron emission is  $2.7 \times 10^{23} \text{ cm}^{-3}$  for PXE and  $4.0 \times 10^{23} \text{ cm}^{-3}$  for water. The response function for  $10^6$  initial  $\gamma$ 's generated in the liquid scintillator volume, and for  $10^7$   $\gamma$ 's generated in the water layer of 100 cm, are shown in Fig. 4. The ratio of the volumes of PXE and water where the  $\gamma$ -events were simulated is 1 : 7; the difference in densities of hydrogen atoms capturing neutrons is small ( $5.1 \times 10^{22} \text{ cm}^{-3}$  for PXE and  $6.7 \times 10^{22} \text{ cm}^{-3}$  for water); hence the response function in Fig. 4 corresponds to practically equal probabilities for the non-Paulian transitions for nucleons in  $^{12}C$  and  $^{16}O$  nuclei. The response function of the CTF2 to the  $\gamma$ 's of 2.2 MeV energy was obtained using the MC model. The shift in the positions of the peaks from 2.2 MeV toward lower energies is a result of the ionization quenching of Compton electrons with a low energy.

The background in the 1.7-2.5 MeV region is a linear function of energy (Fig. 4). Because the peak position is well known, the maximum likelihood method was used to define the intensity of the peak corresponding to the 2.2 MeV  $\gamma$ . Experimental background was modeled as a linear function plus the additional contributions of the response functions for 2.2 MeV  $\gamma$  originating from the PXE

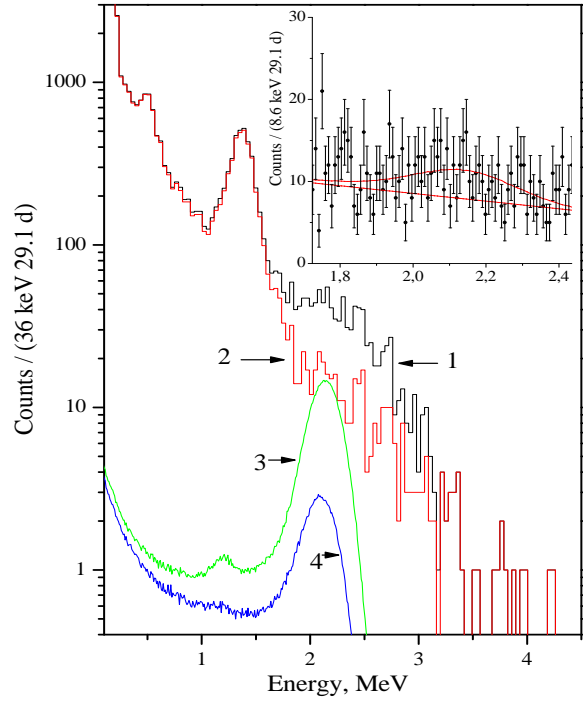


**Fig. 4.** Background energy spectra of the 4.2 ton Borexino CTF2 detector measured over 29.1 days: (1) with muon veto, radial cut ( $R \leq 100$  cm) and  $\alpha/\beta$  discrimination applied; (2) pairs of correlated events (with time interval  $\Delta t \leq 8.2$  ms between signals) are removed; (3) the expected response functions of the detector for  $\gamma$ 's with energy 2.2 MeV due to  $(n, p)$ -capture in the scintillator and (4) in the water. Corresponding mean lifetimes for the  $^{12}C \rightarrow ^{11}\tilde{C} + n$  and  $^{16}O \rightarrow ^{15}\tilde{O} + n$  decays are  $\tau_{lim} = 3.7 \cdot 10^{26}$  y. In the inset the fitting function in the energy interval 1.7–2.5 MeV is shown.

and water. The results of fitting are shown in the inset to Fig. 4. The minimum value of  $\chi^2 = 83.9/90$  corresponds to the total of 100  $\gamma$  events inside LS. For the 90% confidence level, the corresponding limiting number of  $\gamma$  originating from the scintillator is 260. Taking into account the efficiency of the radial cut  $\epsilon_R = 0.80$ , the total number of captured neutrons in the CTF2 can be limited by  $N \leq 2.7n/(d \cdot t)$ . This value is close to the expected rate of neutrons production by muons  $N \approx 1n/(d \cdot t)$  [38].

Finally, the limit on PEP violating transitions of nucleons in  $^{12}C$  and  $^{16}O$  nuclei with neutron emission is

$$\tau(^{12}C(^{16}O) \rightarrow ^{11}\tilde{C}(^{15}\tilde{O}) + n) \geq 3.7 \times 10^{26} \text{ y (90\% c.l.).} \quad (18)$$

This result is 6 orders of magnitude stronger than the one obtained through searching for neutron emission in Pb :  $\tau(\text{Pb} \rightarrow \tilde{Pb} + n) \geq 1.0 \cdot 10^{20} \text{ y (68\% c.l.) [14].}$



#### 4.5 Limits on non-Paulian $\beta^-$ transitions in $^{12}\text{C}$ :

$$^{12}\text{C} \rightarrow ^{12}\tilde{\text{N}} + e^- + \bar{\nu}.$$

The nucleus  $^{12}\text{N}$  is unstable; it decays via  $^{12}\text{N} \rightarrow ^{12}\text{C} + e^+ + \nu$  with an energy release of  $Q = 17.3$  MeV. The inverse process  $^{12}\text{C} \rightarrow ^{12}\tilde{\text{N}} + e^- + \bar{\nu}$  is possible if the binding energy of the non-Paulian nucleus  $E_b(^{12}\tilde{\text{N}})$  is increased in comparison to the binding energy of the normal  $^{12}\text{N}$  nucleus by a value exceeding  $Q$ . The energy released in the reaction  $^{12}\text{C} \rightarrow ^{12}\tilde{\text{N}} + e^- + \bar{\nu}$  is

$$Q = m_n - m_p - m_e - E_b(^{12}\text{C}) + E_b(^{12}\tilde{\text{N}}). \quad (19)$$

The value of  $E_b(^{12}\tilde{\text{N}})$  can be approximated by  $E_b(^{12}\tilde{\text{N}}) \simeq E_b(^{12}\text{N}) + E_p(S_{1/2}, ^{12}\text{N}) - S_p(^{12}\text{N})$ . The separation energy of the proton in  $^{12}\text{N}$  has a very low value,  $S_p(^{12}\text{N}) = 0.6$  MeV. The value of  $E_p(S_{1/2}, ^{12}\text{N})$  can be approximated by the mean value of the binding energies on the  $S_{1/2}$  shell for two neighboring nuclei:  $E_p(S_{1/2}, ^{12}\text{N}) \simeq 0.5 \cdot (E_p(S_{1/2}, ^{12}\text{C}) + E_p(S_{1/2}, ^{16}\text{O})) = 36.8$  MeV. Hence, the expected value of  $Q$  is 18.9 MeV.

The shape of the  $\beta^-$  spectrum with end-point energy 18.9 MeV is shown in Fig. 5. The limit on the probability of this transition was based on the fact of observing no events with  $E_e \geq 4.5$  MeV not accompanied by a muon veto signal. As noted above, it is necessary to take into account the probability  $\eta(E_e)$  of the muon veto triggering for the high energy events in scintillator. The obtained efficiency of detection of electrons with energies  $E_e > 4.5$  MeV is  $\Delta\varepsilon = 0.31$ . The limit on the lifetime of neutrons ( $N_n=4$ ) in  $^{12}\text{C}$  with respect to the transitions violating the PEP is

$$\tau(^{12}\text{C} \rightarrow ^{12}\tilde{\text{N}} + e^- + \bar{\nu}) \geq 7.6 \cdot 10^{27} \text{ y (90\% c.l.)}. \quad (20)$$

This result is 3 orders of magnitude stronger than the one obtained by NEMO-2,  $\tau(^{12}\text{C} \rightarrow ^{12}\tilde{\text{N}} + e^- + \bar{\nu}) \geq 3.1 \cdot 10^{24} \text{ y (90\% c.l.)}$  [11].

The data available from the LSD detector [39] situated in the tunnel under Mont Blanc allows obtaining a qualitative limit for this decay comparable to ours. In [15], it is claimed that only 2 events were observed with energies higher than 12 MeV during 75 days of data taking with the detector loaded with 7.2 tonnes of scintillator, containing  $3 \times 10^{29}$   $^{12}\text{C}$  nuclei. The upper limit that can be obtained using formula (8) with these data (with  $S_{lim}=5.91$  events for 90% c.l. and detection efficiency  $\Delta\varepsilon = 0.23$ ) is  $\tau(^{12}\text{C} \rightarrow ^{12}\tilde{\text{N}} + e^- + \bar{\nu}) \geq 9.5 \cdot 10^{27} \text{ y (90\% c.l.)}$ . We did not cite this approximate result in table 2, because the exact calculation requires precise knowledge of efficiency of the LSD detector.

#### 4.6 Limits on non-Paulian $\beta^+$ transitions in $^{12}\text{C}$ :

$$^{12}\text{C} \rightarrow ^{12}\tilde{\text{B}} + e^+ + \nu.$$

The energy release for this reaction,  $Q = 17.8$  MeV, was calculated by assuming that the binding energy of the

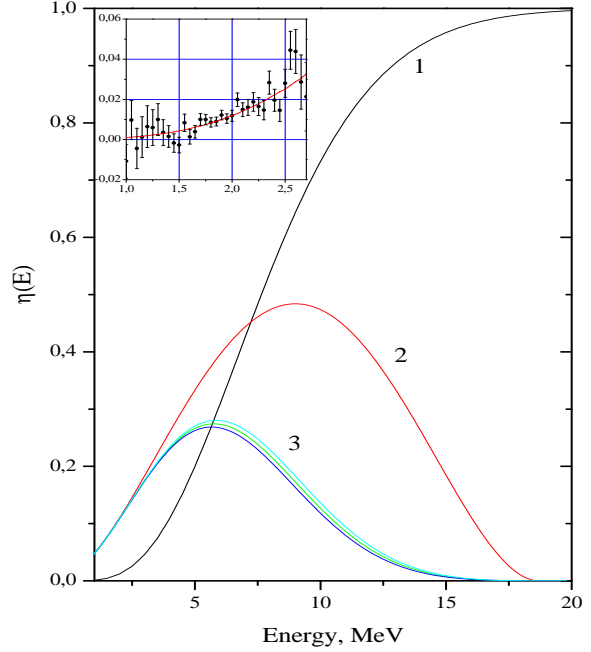


**Fig. 5.** Probability of identification of an event with energy  $E$  in the scintillator by the muon veto  $\eta(E)$  (1). The  $\beta$  spectra of  $^{12}\text{C} \rightarrow ^{12}\tilde{\text{N}} + e^- + \bar{\nu}_e$  without (2) and with (3) suppression by the muon veto are also shown in arbitrary units. In the inset, the  $\eta(E)$  function together with the experimental data taken with the radon source are presented. The tagged events of  $^{214}\text{Bi}$ - $^{214}\text{Po}$  at the energy  $E=1.9$  MeV are 'seen' by the muon veto system with an efficiency of  $\eta(1.9 \text{ MeV}) = 0.01$ .

neutron in  $S_{1/2}$ - shell in  $^{12}\text{B}$  nuclei is close to the experimentally found value for the nuclei  $^{11}\text{B}$ :  $E_n(S_{1/2}, ^{12}\text{B}) \simeq E_n(S_{1/2}, ^{11}\text{B}) = 34.5$  MeV. The end-point energy of the  $\beta^+$  spectrum is 16.8 MeV, but the spectrum is shifted towards higher energies by  $\simeq 0.8$  MeV due to the registering of annihilation quanta. The efficiency of the  $^{12}\text{C} \rightarrow ^{12}\tilde{\text{B}} + e^+ + \nu$  transition detection with energy release  $E > 4.5$  MeV is  $\varepsilon_{\Delta E} = 0.31$ . The lower limit on the lifetime of the proton in the  $^{12}\text{C}$  nuclei is then

$$\tau(^{12}\text{C} \rightarrow ^{12}\tilde{\text{B}} + e^+ + \nu) \geq 7.7 \cdot 10^{27} \text{ y (90\% c.l.)} \quad (21)$$

The limits obtained by the NEMO collaboration for this reaction are 3 orders of magnitude weaker:  $\tau(^{12}\text{C} \rightarrow ^{12}\tilde{\text{B}} + e^+ + \nu) \geq 2.6 \cdot 10^{24} \text{ y (90\% c.l.)}$  [11].

The final results for different PEP violation transitions are shown in table 2 in comparison with previous results.

## 5 Conclusions

Using the unique features of the Borexino Counting Test Facility – the extremely low background, large scintillator mass of 4.2 tonnes, carefully designed muon-veto system and low energy threshold – new limits on non-Paulian

**Table 2.** Mean lifetime limits,  $\tau_{lim}$  (at 90% C.L.), for non-Paulian transitions in the CTF2.  $E_0$  is the average energy of particles, or end-point energy in the case of  $\beta^\pm$ -transitions;  $\Delta E$  is the energy window of CTF2 in which decays were searched for;  $\varepsilon_{\Delta E}$  is the detection efficiency;  $S_{lim}$  the excluded number of events in the CTF2 spectrum.

Channel	$E_0$ , (MeV)	$\Delta E$ (MeV)	$\varepsilon_{\Delta E}$	$S_{lim}$	$\tau_{lim}$ (y) 90% c.l.	Previous limits
$^{12}\text{C} \rightarrow ^{12}\tilde{\text{C}} + \gamma$	17.5	$\geq 4.5$	$4.3 \cdot 10^{-2}$	2.44	$2.1 \cdot 10^{27}$	$4.2 \cdot 10^{24}$ [11]
$^{16}\text{O} \rightarrow ^{16}\tilde{\text{O}} + \gamma$	21.8	$\geq 4.5$	$5.6 \cdot 10^{-3}$	2.44	$2.1 \cdot 10^{27}$	$2.7 \cdot 10^{27}$ [10]
$^{12}\text{C} \rightarrow ^{11}\tilde{\text{B}} + p$	4.8-8.2	2.0-4.7	$0.68 \times 0.8$	130	$5.0 \cdot 10^{26}$	$1.7 \cdot 10^{25}$ [12]
$^{12}\text{C}(^{16}\text{O}) \rightarrow ^{11}\tilde{\text{C}}(^{15}\tilde{\text{O}}) + n$	2.2	1.7-2.5	0.8	260	$3.7 \cdot 10^{26}$	$1.0 \cdot 10^{20}$ [14]
$^{12}\text{C} \rightarrow ^8\tilde{\text{B}}e + \alpha$	2.0	0.07-0.23	0.68	3300	$6.1 \cdot 10^{23}$	-
$^{12}\text{C} \rightarrow ^{12}\tilde{\text{N}} + e^- + \bar{\nu}_e$	18.9	$\geq 4.5$	0.31	2.44	$7.6 \cdot 10^{27}$	$3.1 \cdot 10^{24}$ [11]
$^{12}\text{C} \rightarrow ^{12}\tilde{\text{B}} + e^+ + \nu_e$	17.8	$\geq 4.5$	0.31	2.44	$7.7 \cdot 10^{27}$	$2.6 \cdot 10^{24}$ [11]

transitions of nucleons from the  $P$ -shell to the  $1S_{1/2}$ -shell in  $^{12}\text{C}$  and  $^{16}\text{O}$  with the emission of  $\gamma, n, p, \alpha$  and  $\beta^\pm$  particles have been obtained:

$$\begin{aligned} \tau(^{12}\text{C} \rightarrow ^{12}\tilde{\text{C}} + \gamma) &> 2.1 \cdot 10^{27} \text{ y}, \\ \tau(^{16}\text{O} \rightarrow ^{16}\tilde{\text{O}} + \gamma) &> 2.1 \cdot 10^{27} \text{ y}, \\ \tau(^{12}\text{C} \rightarrow ^{11}\tilde{\text{B}} + p) &> 5.0 \cdot 10^{26} \text{ y}, \\ \tau(^{12}\text{C}(^{16}\text{O}) \rightarrow ^{11}\tilde{\text{C}}(^{15}\tilde{\text{O}}) + n) &> 3.7 \cdot 10^{26} \text{ y}, \\ \tau(^{12}\text{C} \rightarrow ^8\tilde{\text{B}}e + \alpha) &> 6.1 \cdot 10^{23} \text{ y}, \\ \tau(^{12}\text{C} \rightarrow ^{12}\tilde{\text{N}} + e^- + \bar{\nu}_e) &> 7.6 \cdot 10^{27} \text{ y} \end{aligned}$$

and  
 $\tau(^{12}\text{C} \rightarrow ^{12}\tilde{\text{B}} + e^+ + \nu_e) > 7.7 \cdot 10^{27} \text{ y}$ , all with 90% C.L.

Comparing these values with the data of table 2, one can see that these limits for non-Paulian transitions in  $^{12}\text{C}$  with  $\gamma$ -,  $p$ -,  $n$ -,  $\alpha$ -, and  $\beta^\pm$ - emissions are the best to date. The limits on the  $\beta^\pm$  non-Paulian transitions in  $^{12}\text{C}$  are comparable to those that can be obtained with the data of the LSD detector [15],[39] and the limit on non-Paulian transition in  $^{16}\text{O}$  with  $\gamma$  emission is comparable to the result obtained using Kamiokande data [10].

## References

1. F. Reines, H.W. Sobel, Phys. Rev. Lett. 32 (1974) 954
2. B.A. Logan, A. Ljubcic, Phys. Rev. C20 (1979) 1957
3. R.D. Amado, H. Primakoff, Phys. Rev. C22 (1980) 1338
4. A.Yu. Ignatiev, V.A. Kuzmin, Sov. J. Nucl. Phys. 461 (1987) 786
5. O.W. Greenberg, R.N. Mohapatra, Phys. Rev. Lett. 59 (1987) 2507, 62 (1989) 712, Phys. Rev. D39 (1989) 2032
6. L.B. Okun, JETP Lett. 46 (1987) 529
7. A.B. Govorkov, Phys. Lett. A137 (1989) 7
8. L.B. Okun, Physics Uspekhi, 158 (1989) 293 (Sov. Phys. Usp. 32 (1989) 543)
9. L.B. Okun, Comments Nucl. Part. Phys., 19 (1989) 99
10. Y. Suzuki et al., Phys. Lett. B311 (1993) 357
11. NEMO coll., R. Arnold et al., Europ. Phys.J. A6 (1999) 361
12. H. Ejiri, H. Toki, Phys. Lett. B306 (1993) 218
13. R. Bernabei et al., Phys. Lett. B408 (1997) 439

14. T. Kishimoto et al., J. Phys. G18 (1992) 443
15. D. Kekez, A.A. Ljubičić, B.A. Logan, Nature 348 (1990) 224
16. D. Miljanić et al., Phys. Lett. B252 (1990) 487
17. Borexino Collaboration, H.O. Back et al., Phys. Lett. B525 (2002) 29
18. Borexino Collaboration, H.O. Back et al., Phys. Lett. B563 (2003) 35
19. Borexino Collaboration, H.O. Back et al., Phys. Lett. B563 (2003) 23
20. Borexino Collaboration, H.O. Back et al., JETP Lett. 78 (2003) 261
21. Borexino Collaboration, G. Alimonti et al., Astropart. Phys. 16 (2002) 205
22. Borexino Collaboration, G. Alimonti et al., Nucl. Instrum. Meth. A406 (1998) 411; Astropart. Phys. 8 (1998) 141; Phys. Lett. B422 (1998) 349
23. Borexino Collaboration, G. Alimonti et al., Nucl. Instrum. Meth. A440 (2000) 360
24. Borexino coll., A high density and high-flash-point organic liquid scintillator for applications in low-energy particle-astrophysics experiments, to be published
25. J.B. Birks, Proc. Phys. Soc. A64 (1951) 874
26. J.M. Los Arcos, F. Ortiz, Comp. Phys. Comm. 103 (1997) 83
27. O.Ju. Smirnov, Instr. and Exp. Technique 46 (2003) 327
28. M. Johnson et al., Nucl. Instrum. Meth. A414 (1998) 459
29. S.L. Belostotski et al., Sov. J. Nucl. Phys. 41 (1985) 903
30. G. Audi, A.H. Wapstra, Nucl. Phys. A595 (1995) 409
31. L. Lapikas et al., Phys. Rev. C61 (2000) 064325
32. Y. Kamyshkov, E. Kolbe, Phys. Rev. D66 (2002) 010001
33. W.R. Nelson, H. Hirayama, D.W.O. Rogers, SLAC-Report-265, Stanford, 1985
34. A. Derbin, A. Ianni, V. Muratova, O. Smirnov, A Simple Monte-Carlo model of the CTF detector. Borexino Internal Note, December, 2003
35. M. Neff, Diploma thesis, Technische Universität München, 1996
36. G.J. Feldman, R.D. Cousins, Phys. Rev. D57 (1998) 3873
37. J.H. Lee, C.S. Lee, Nucl. Instrum. Meth. A402 (1998) 147
38. F.F. Khalchukov et.al., Nuovo Cim. 18 (1995) 517
39. M. Aglietta et al., Nuovo Cim. C9 (1986) 185